20 January 1949

THE EXPERIMENTAL AND THEORETICAL PRESSURE DISTRIBUTION AND NORMAL FORCE OF A CONE-CYLINDER CONFIGURATION AT A MACH NUMBER OF 1.93

By W. H. Dorrance
W. H. Dorrance

Approved F. W. Ross
F. W. Ross

AERONAUTICAL RESEARCH CENTER

WILLOW RUN AIRPORT YPSILANTI, MICHIGAN

SUMMARY OF CONCLUSIONS

The results of pressure distribution tests on a cone-cylinder model at a Mach Number of 1.93 are presented in the form of pressure coefficient and normal force coefficient as a function of angle of attack. On the basis of these results the following conclusions are drawn.

1. The cylindrical portion of the body contributes between 35% and 55% of the total normal force of the configuration.

2. The linearized theory predicts a normal force variation with angle of attack in good agreement with the experimental results.

3. The trend of pressure coefficient variation versus axial distance for each meridian plane agrees with linearized theory, but the magnitudes of pressure coefficient disagree over the after portion of the cylinder. It is noted that this may possibly be due to impinging of tunnel interference shock waves.

SYMBOLS

c_n = section normal force coefficient

C_N = total normal force coefficient

$$= \frac{1}{L}\int_0^{\ell} c_n \, dx$$

C_p = $\dfrac{P - Pa}{q}$ = pressure coefficient

D = drag force

l = model total length

L = lift force

M = Mach Number

N = normal force

p = local surface static pressure

p_a = ambient static pressure

p_o = total stagnation pressure

q = $\dfrac{\rho V^2}{2}$ = free stream dynamic pressure

V = free stream velocity

Greek symbols

α = angle of attack

θ = meridian plane (0^o, 45^o, 90^o, 135^o, 180^o)

ρ = free stream density

ϕ = roll angle (0^o, 180^o)

INTRODUCTION

A series of pressure distribution tests on a sequence of supersonic configurations is being run at Mach Number 1.93 to provide basic aerodynamic data. Included in these tests is a pressure survey on a configuration consisting of a conical nose and cylindrical afterbody. The model was tested at positive and negative angles of attack, and the data so obtained is reduced in this report to plots of pressure coefficient and normal force coefficient. Theoretical results of such a configuration are compared with the experimental results where possible.

DISCUSSION

A cone-cylinder body of revolution was tested in the University of Michigan supersonic wind tunnel at the Aeronautical Research Center at a Mach number of 1.93. The model was constructed of stainless steel and provided with 28 surface pressure taps located on the cylindrical section as shown in Figure 1. The vertex angle of the conical nose was specified as 20° so that results previously obtained for a 20° cone reported in Reference 1 could be used for this section of the body.

Readings were taken at 0°, 2°, 4°, 6°, 8°, and 10° angles of attack at 0° and 45° roll about the axis of symmetry of the model. Such a procedure yields pressure readings in the five meridian planes $\theta = 0^{\circ}$, 45°, 90°, 135°, and 180° at both positive and negative angles of attack. Figure 2 illustrates this procedure.

A Schlieren photograph was taken for each angle of attack. A vertical plumb line appears as a reference line in each photograph from which the actual angle of attack can be read. Figure 3 is a typical Schlieren photograph taken at an angle of attack of 0°.

The value of pressure coefficient, C_p, was obtained for each orifice using the equation given below by the wind tunnel group and presented as test data.

$$C_p = \frac{P/P_0 - P_a/P_0}{q/P_0} \qquad (1)$$

$$P/P_0 = P/P_a \times P_a/P_0$$

= value determined from reading the manometer bank

$\frac{p_a}{p_o}$ = value for each station taken from a plot of $\frac{p_a}{p_o}$ along tunnel centerline in region of model

$\frac{q}{p_o}$ = mean value taken for convenience of calculation.

This introduces an error of less than 1% in C_p in most cases.

Using a graphical method of integration the normal force on the cylindrical section of the configuration was obtained from the values of C_p determined as above. The procedure used is outlined below. Consider a typical cross section of the cylindrical portion of the model perpendicular to the model centerline as sketched below.

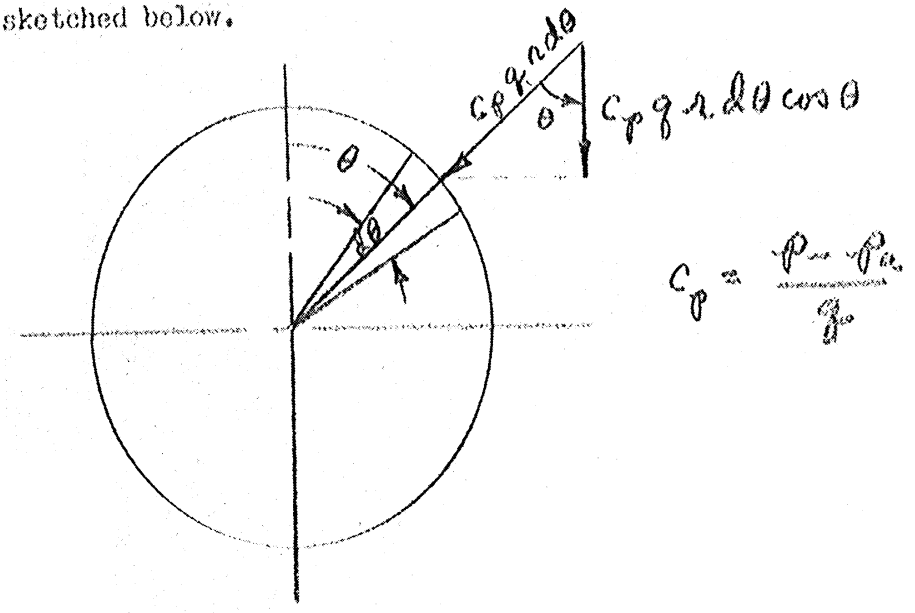

NOW:

$$C_n = \int_0^{2\pi} \frac{(p - p_a)}{q A_{max.}} \cos\theta \, r \, d\theta$$

OR:

$$C_n = \frac{2r}{A_{max}} \int_0^{\pi} C_p \cos\theta \, d\theta$$

hence

$$c_n = \frac{2}{\pi R} \int_0^{\pi} C_p \cos\theta \, d\theta \qquad (2)$$

Then

$$C_N = \int_0^{\ell} c_n \, dx \qquad (3)$$

The section normal force coefficient was obtained by a method of graphical integration based on equation (2) for each seven longitudinal stations along the cylindrical section at angles of attack of 2°, 4°, 6°, 8° and 10°. Using the section normal force coefficients determined by equation (2) the total normal force coefficient is determined graphically for the cylindrical section using equation (3). Figure 4 presents a typical plot of c_n versus x used to determine the total normal force coefficient of the cylindrical section at an angle of attack of 6°.

On the basis of the normal force coefficients of the cylindrical section determined in this manner it is evident that the cylindrical section definitely contributes a normal force and hence a lift and drag force. Figure 5 illustrates a normal force coefficient curve versus angle of attack for the cylindrical section alone compared to similar curves for the cone nose alone and for the complete configuration. These curves will be discussed separately in the following text.

The normal force coefficient for the conical nose was obtained from 20° cone data previously reported in Reference 1. The lift and drag coefficient curves versus angle of attack were determined from pressure distribution data in Reference 1. The normal force for the cone nose was determined using the familiar expression below.

$$N = L\cos\alpha + D\sin\alpha \qquad (4)$$

Once the cone nose normal force, N, was determined the normal force coefficient was calculated and plotted for comparison in Figure 5. The curve is approximately linear as is predicted by theory.

The normal force for the complete cone-cylinder configuration is shown in Figure 5 as a function of angle of attack. Because the normal force coefficients for the 20° cone nose and the cylindrical components were both based on the cylindrical base area the complete normal force coefficient is the sum of the separate component normal force coefficients. This total normal force coefficient curve departs from the linear characteristic variation of the cone nose because of the curvative present in the curve representing the component normal force coefficient of the cylindrical section. This curvature will be discussed in the following.

The value of $\frac{dC_N}{d\alpha}$ for the cone-cylinder model was calculated using the linearized theory outlined in Reference 2. Using this value, the curve of C_N versus α was plotted for comparison purposes on Figure 5. It can be seen that good agreement exists between experiment and theory in the range of angles considered. This was to be expected because the linearized theory should give good results for this comparatively low Mach Number of 1.93.

To assist in calculating the values of section normal force coefficient C_N and to provide a common parameter to compare with theory, curves of pressure coefficient C_p versus axial length along the cylindrical section were prepared for the five meridian planes represented in Figure 2 at angles of attack of 0°, 2°, 4°, 6°, 8° and 10°. Figures 6,7,8,9, 10 and 11 present this data in graphical form.

The theoretical value of pressure coefficient for the cone-cylinder model at zero angle of attack was obtained through using the linearized theory outlined in Reference 2. These values are plotted in Figure 6 and compared with the experimental results. Inspection of this figure reveals that the experimental results depart somewhat from the theoretical magnitudes over the after section of the cylindrical section. The experimental values of pressure coefficient as read at orifice stations (6) and (7) indicate static pressure exceeding free stream static pressure. The theory indicates that the body static pressure nowhere exceeds free-stream static pressure. Tests run on a similar configuration at M = 1.47, 1.72 and 2.00 reported in Reference 3 found close agreement between experiment and theory. On the basis of these results and the theoretical results an investigation into this discrepancy was conducted.

Examination of the Schlieren photographs revealed that shock waves originating at the nozzle test section juncture were impinging on the after region of the cylindrical section of the model. The occurance of these shock waves is reported in the wind tunnel calibration report, Reference 4. Figure 3 is a Schlieren photograph of the model at 10^{o} and illustrates the presence of these shock waves in the vicinity of the model. The location of the point of intersection of these shock waves with the model surface was scaled from Schlieren photographs to determine their region of influence. The shock wave intersections are shown in the following sketch together with the orifice planes in their vicinity. The sketch represents the model at 0^{o} angle of attack.

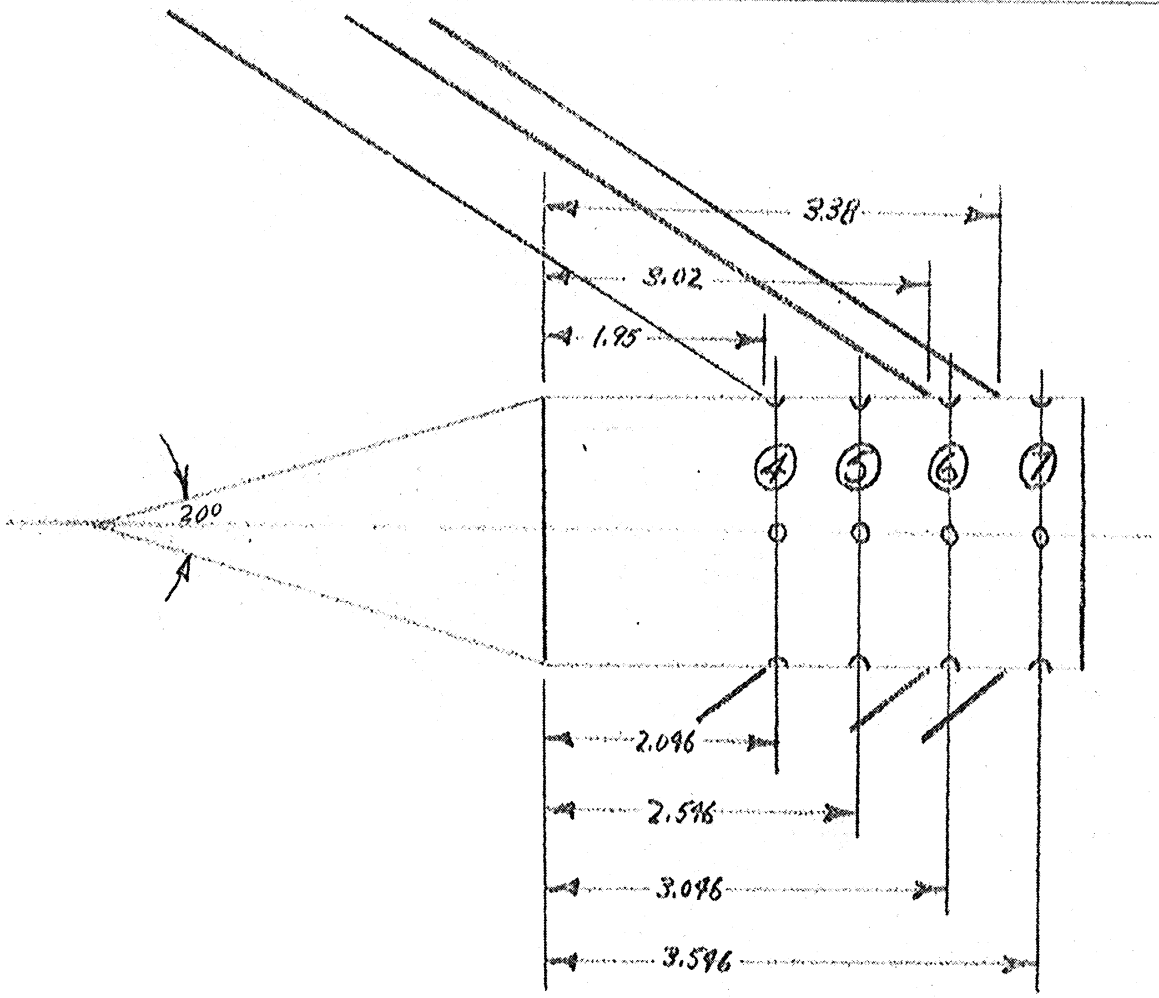

As is shown above, the impinging weak shock waves can influence orifice planes (4), (5), (6) and (7). Examination of Figure 6 reveals that the values of pressure coefficient for these orifice planes is higher than the theory predicts. Part of this increase in pressure coefficient over that predicted by theory is attributed to the interference of the juncture shock waves. These waves influence the static pressure values at the body in two ways. Associated with each shock wave is an inherent jump in static pressure which increases the local value of pressure coefficient over the value to be expected in the absence of the shock waves. In addition to this manifestation the impinging shock waves influence the boundary layer in such a way as to contribute to an additional static pressure increase. Analysis of the Schlieren photographs reveals a tendency towards boundary layer thickening beginning

slightly forward of the foremost impinging shock wave. This boundary layer increase is brought about by the local increase in static pressure which adversely affects the boundary layer momentum. This increased pressure is propagated forward in the subsonic layer thickening the layer in front of the shock wave. Associated with this boundary layer growth is an additional compression in static pressure. This latter phenomenon is represented schematically below.

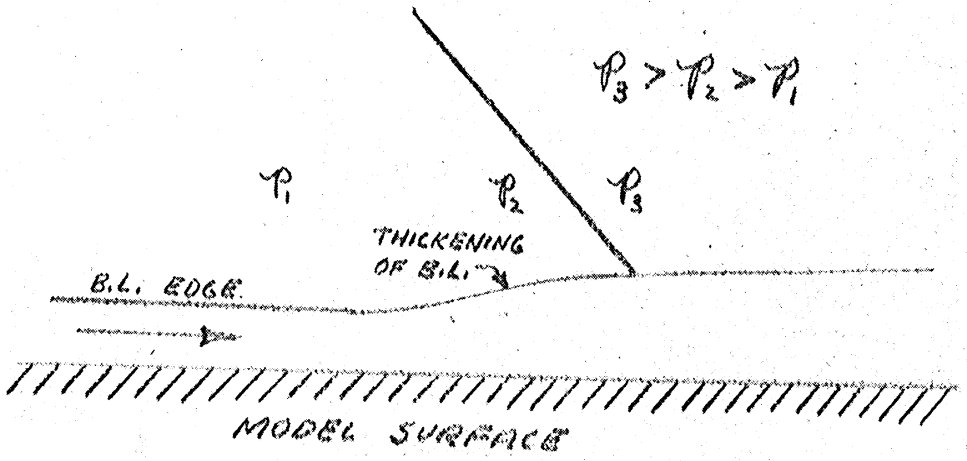

The explanation for the discrepancy in surface static pressure should be valid at all angles of attack. The curvature in the normal force coefficient curve as a function of angle of attack can be explained on the basis of this phenomenon. As the angle of attack increases the nose shock "wave" in the 0° meridian plane or in the "top" plane decreases in strength. Conversely, the nose shock "wave" in the "bottom" plane or 180° meridian plane increases in strength. As a result, the interference shocks when intersecting the nose shock are deflected differently in the two planes. That is, the 0° meridian plane interference shock wave impinges on the upper surface of the cylindrical section of the

model further aft than the 180° meridian plane interference wave impinges the lower surface of the model. The results of this behavior is to increase the static pressure over the aft end of the model in such a manner that the surface integration of pressure as in equation (2) yields a section normal force coefficient that behaves non-linearly with angle of attack at the higher angles of attack.

In preparing the curves of experimental pressure coefficient versus axial station for the five meridian planes at the various angles of attack it was decided to fair smooth curves through the experimental data. Figure 12 presents the curves of pressure coefficient versus axial length for an angle of attack of 6° where the curves are drawn through the experimental points. Comparison of these curves with those curves faired through the experimental points at an angle of attack of 6° shown in Figure 9 reveals that little change in trends or magnitudes is shown. On the basis of this the procedure as followed is deemed as valid as any that could be devised utilizing pressure data.

REFERENCES

1. "Pressure Distribution and Force Coefficients on a 20^{0} Cone Using Experimental and Theoretical Methods", by W. H. Dorrance, University of Michigan, EMB-5.

2. "The Application of the Singularity Method to Finding the Linearized Pressure Distribution Over a Body of Revolution, by W. H. Dorrance, University of Michigan, EMB-9.

3. "Pressure Distributions Over a Cylinder with Conical or Hemispherical Nose", by L.L. Cronvich, APL/JHU TG-10-4, Figure 5 and text discussion.

4. "Final Calibration Report on the Mach 2 Configuration, Excluding Balance System, in the U.M.E.R.I. Supersonic Wind Tunnel", by W. H. Curry, University of Michigan, WTM-45.

CONE - CYLINDER MODEL TESTED AT M=1.93

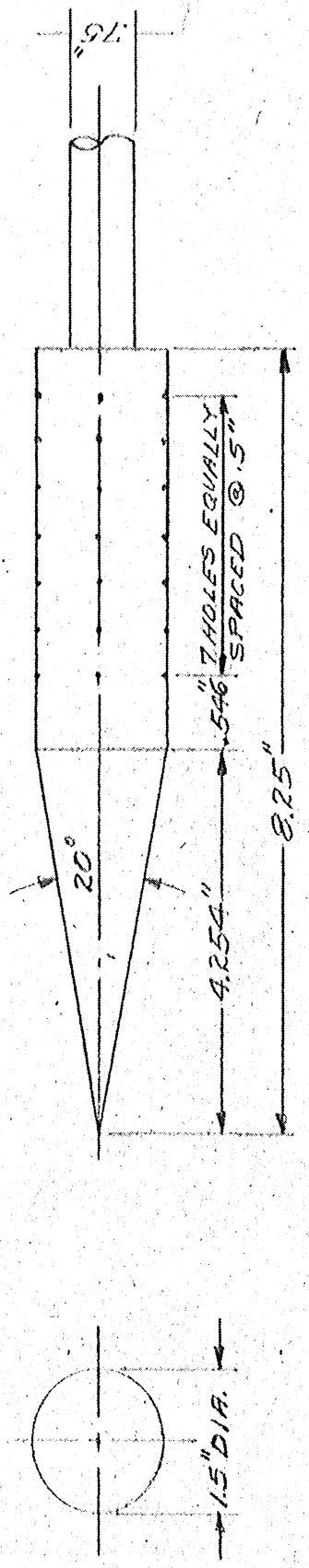

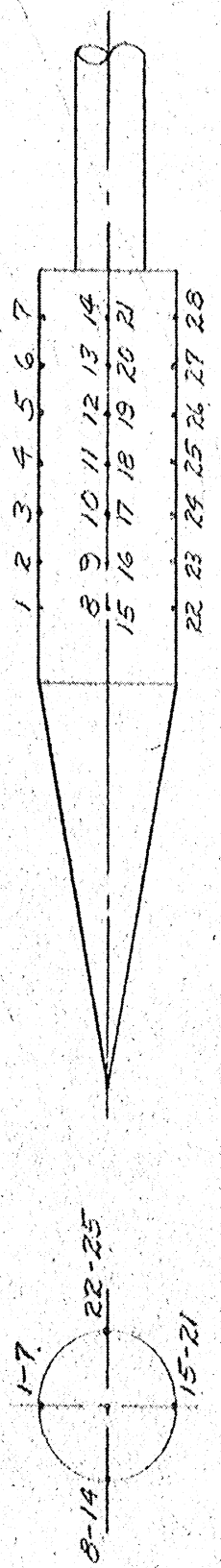

FIGURE 1

TEST PROCEDURE FOR CONE-CYLINDER PRESSURE TESTS AT M=1.93

$\alpha = 0°, 2°, 4°, 6°, 8°, 10°$

FACING DOWNSTREAM

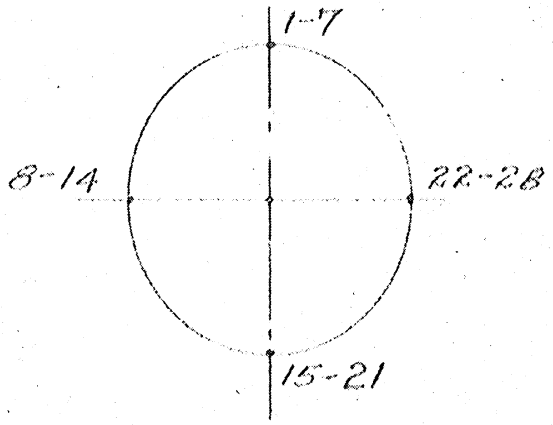

$\phi = 0°$

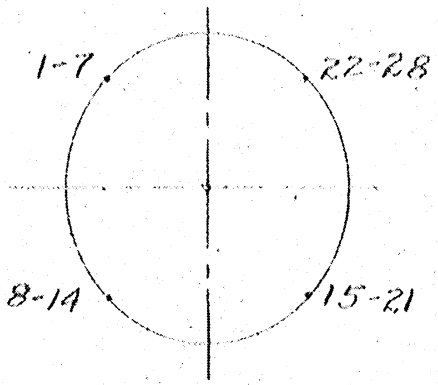

$\phi = 45°$

FIGURE 2

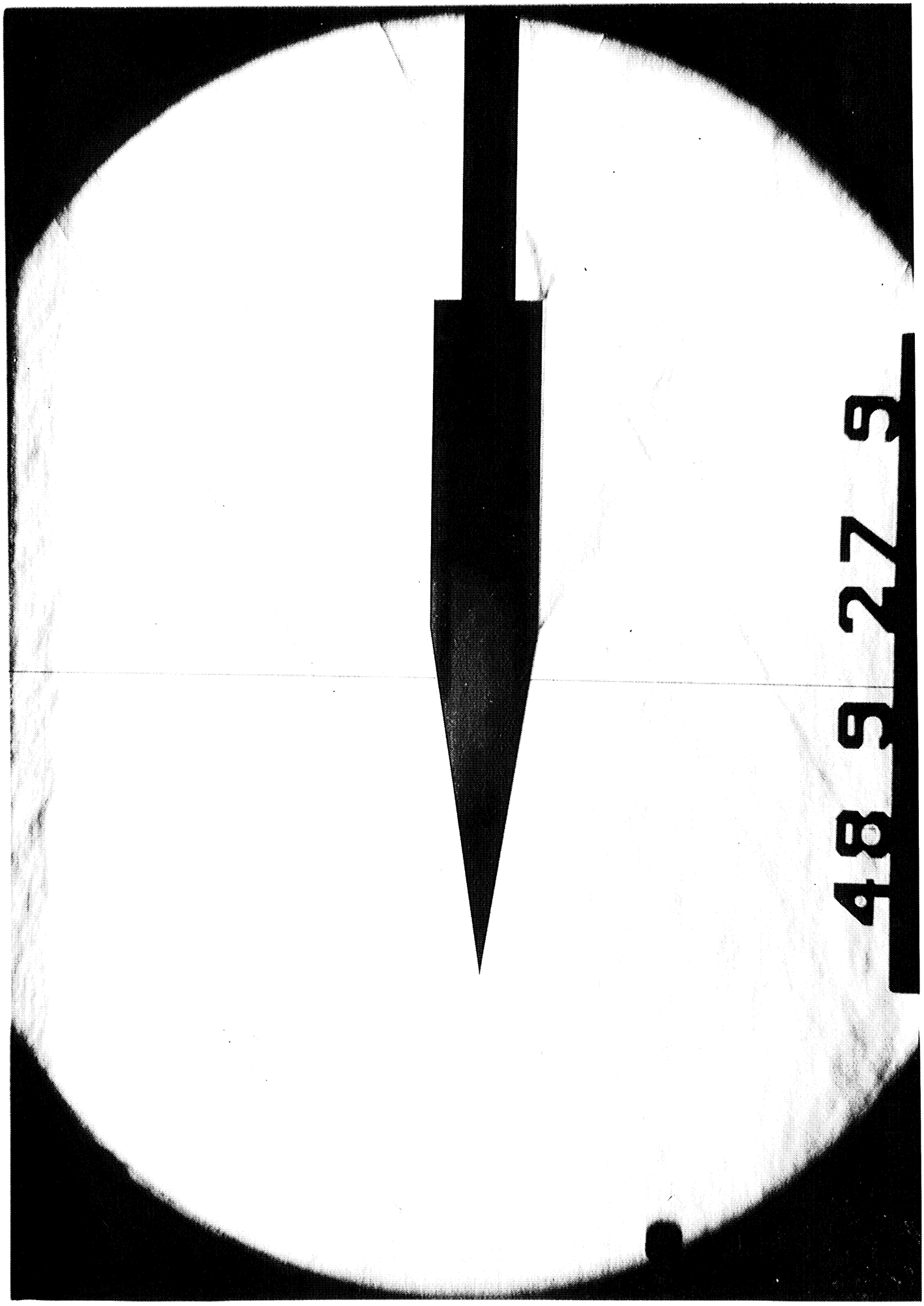

FIGURE 8

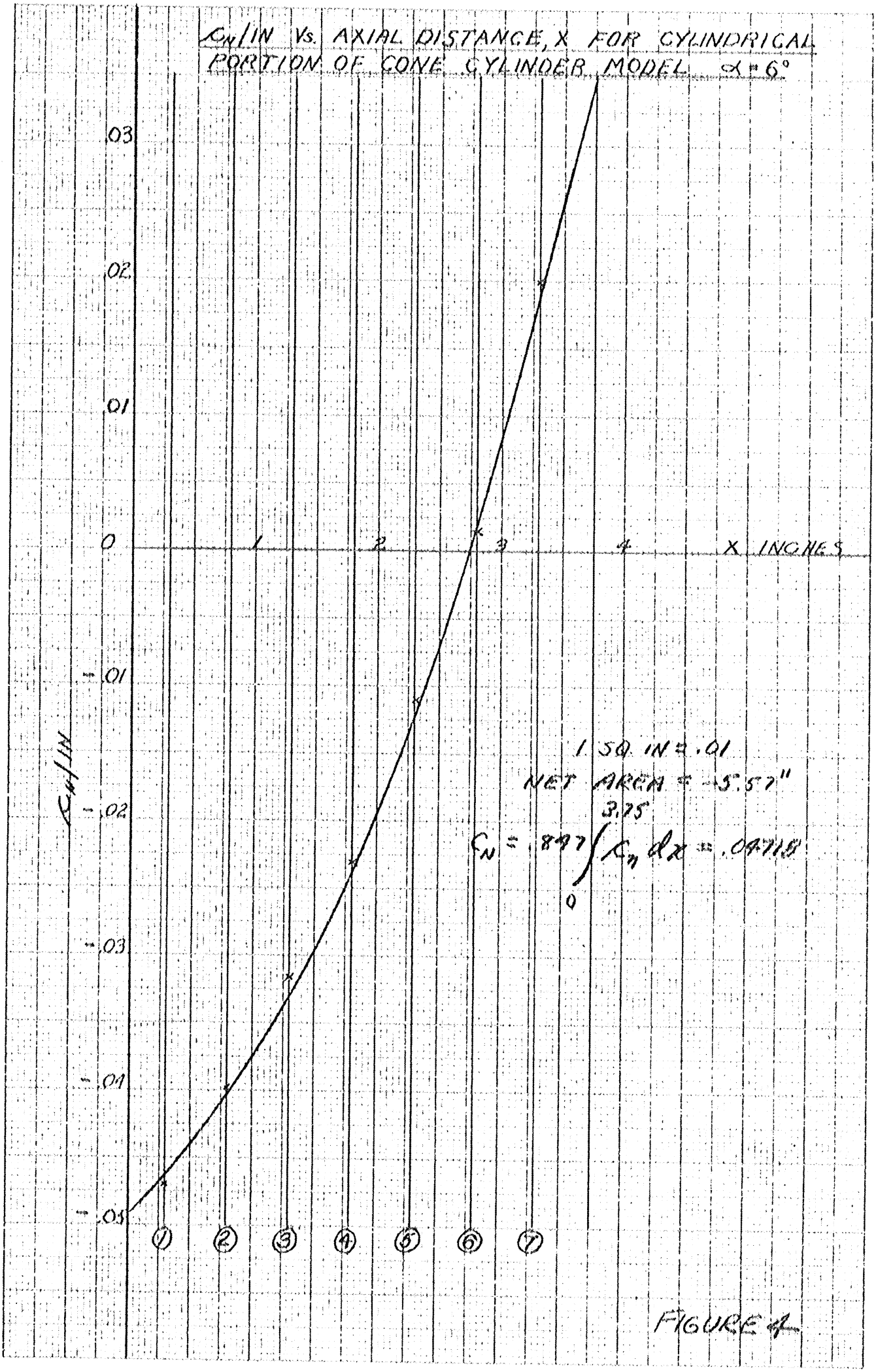
C_N/IN Vs. AXIAL DISTANCE, X FOR CYLINDRICAL PORTION OF CONE CYLINDER MODEL $\alpha = 6°$
.03
.02
.01
0
1
2
3
4
X INCHES
-.01
-.02
-.03
-.04
-.05
C_N/IN
1.50 IN = .01
NET AREA = 5.57"
$C_N = .897 \int_0^{3.75} C_n \, dx = .0471$
①
②
③
④
⑤
⑥
⑦

FIGURE 4

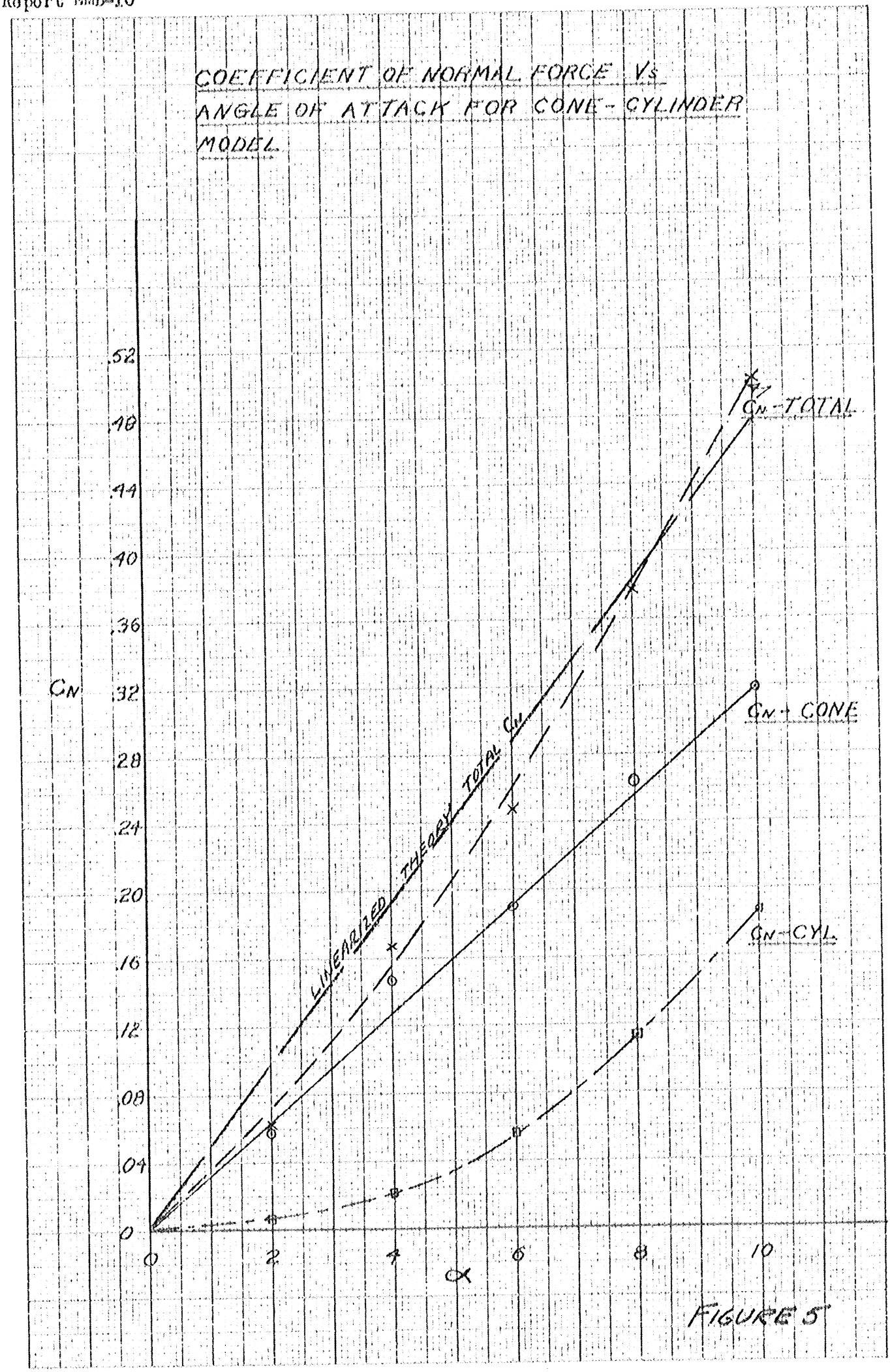
COEFFICIENT OF NORMAL FORCE Vs
ANGLE OF ATTACK FOR CONE-CYLINDER
MODEL
C_N
.52
.48
.44
.40
.36
.32
.28
.24
.20
.16
.12
.08
.04
0
0
2
4
6
8
10
α
C_N - TOTAL
C_N - CONE
C_N - CYL.
LINEARIZED THEORY TOTAL C_N

FIGURE 5

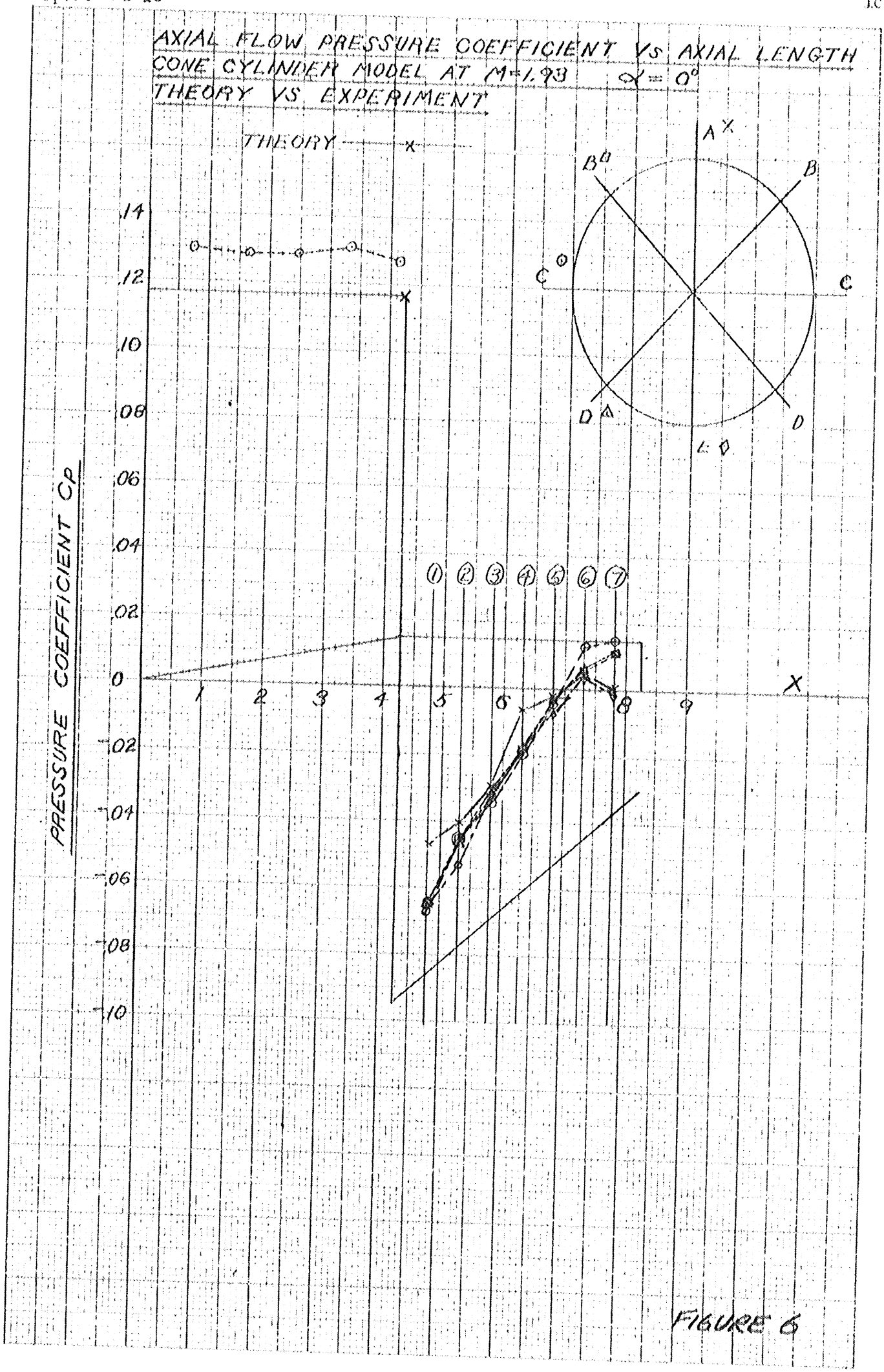
AXIAL FLOW PRESSURE COEFFICIENT VS AXIAL LENGTH
CONE CYLINDER MODEL AT M=1.93 α = 0°
THEORY VS EXPERIMENT
THEORY
PRESSURE COEFFICIENT Cp
.14
.12
.10
.08
.06
.04
.02
0
-.02
-.04
-.06
-.08
-.10
1
2
3
4
5
6
7
8
9
X
A
B
C
D
(1) (2) (3) (4) (5) (6) (7)

FIGURE 6

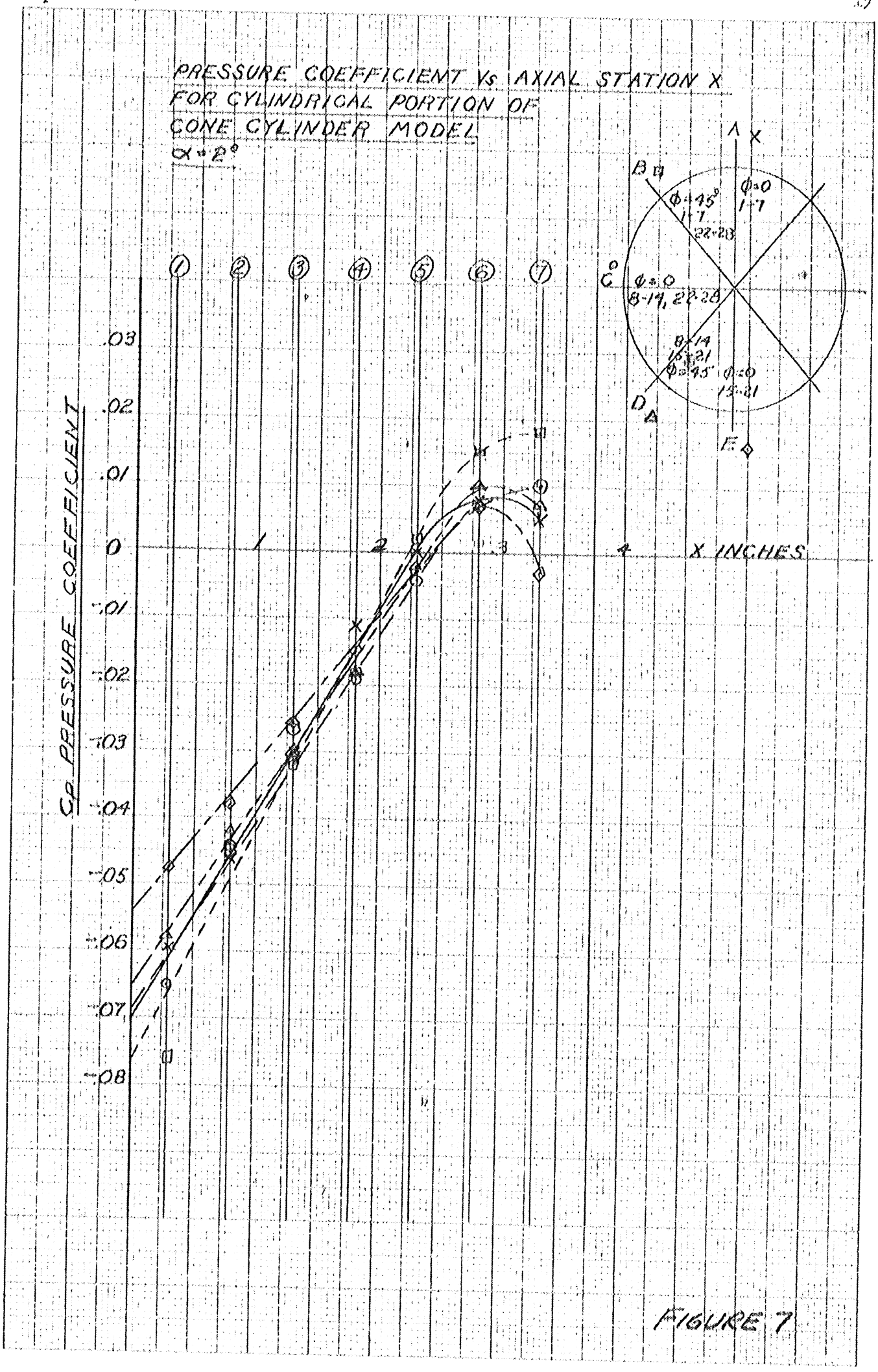
PRESSURE COEFFICIENT Vs AXIAL STATION X
FOR CYLINDRICAL PORTION OF
CONE CYLINDER MODEL
α = 2°
Cp PRESSURE COEFFICIENT
.03
.02
.01
0
-.01
-.02
-.03
-.04
-.05
-.06
-.07
-.08
1
2
3
4
X INCHES
X
B
C
D
E
Φ=45°
Φ=0
1-7
22-28
8-14, 22-28
15-21

FIGURE 7

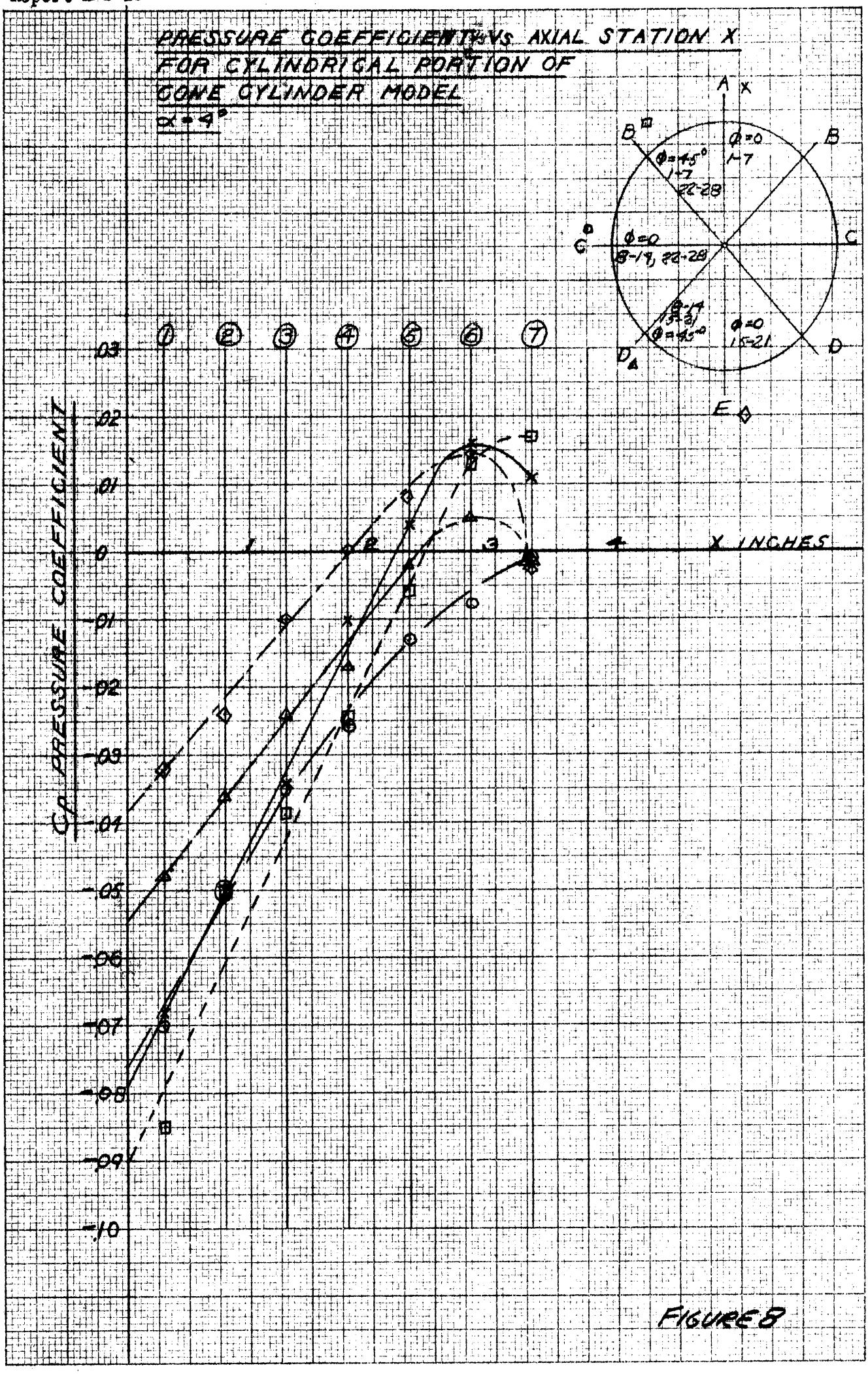

FIGURE 8

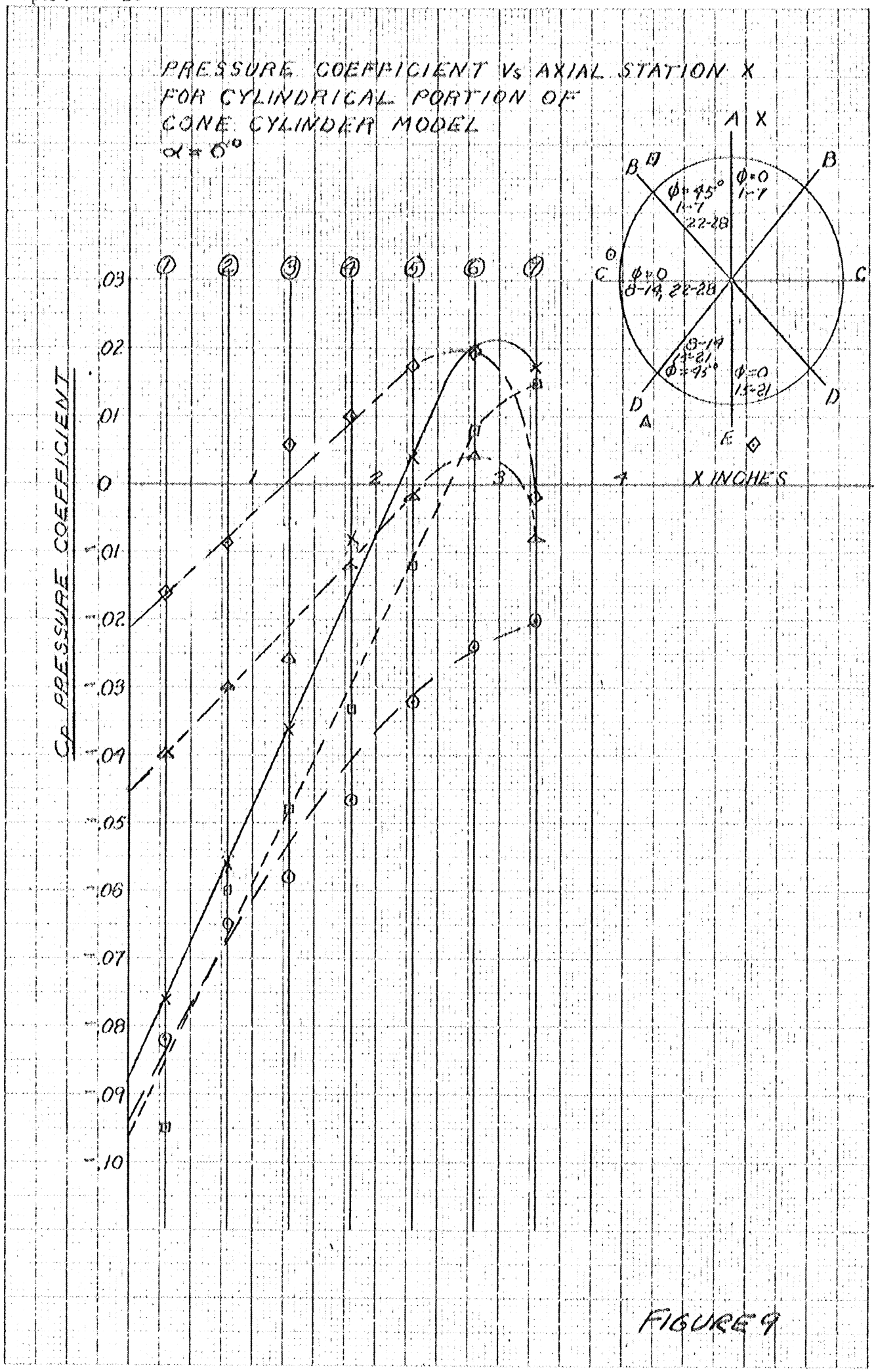
PRESSURE COEFFICIENT Vs AXIAL STATION X
FOR CYLINDRICAL PORTION OF
CONE CYLINDER MODEL
α = 6°
Cp PRESSURE COEFFICIENT
X INCHES
A X
B
C
D
E
φ=0
1-7
φ=45°
1-7
22-28
φ=0
8-14, 22-28
8-14
15-21
φ=90°
φ=0
15-21

FIGURE 9

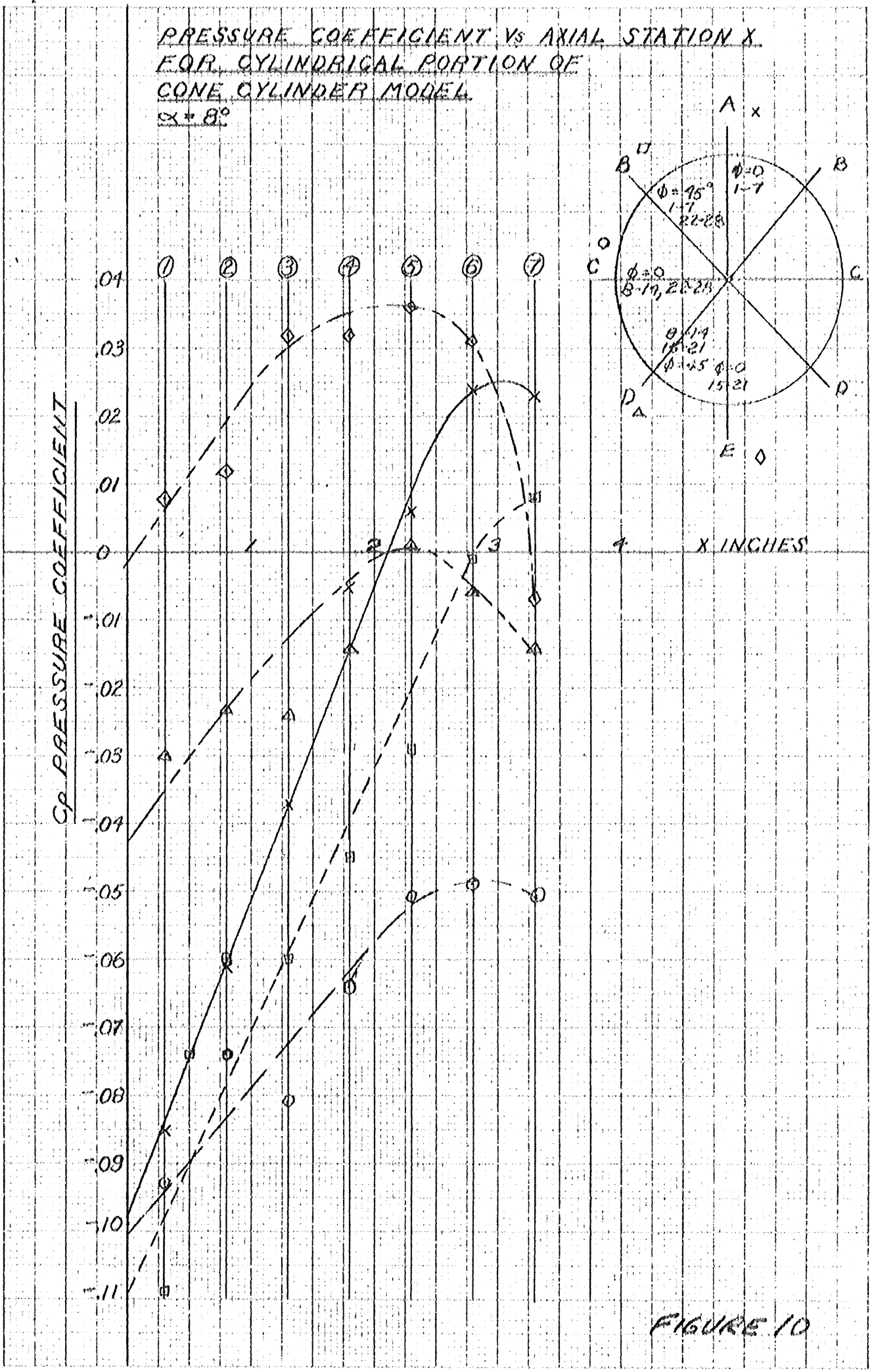
PRESSURE COEFFICIENT Vs AXIAL STATION X
FOR CYLINDRICAL PORTION OF
CONE CYLINDER MODEL
α = 8°
Cp PRESSURE COEFFICIENT
X INCHES
.04
.03
.02
.01
0
-.01
-.02
-.03
-.04
-.05
-.06
-.07
-.08
-.09
-.10
-.11
0
1
2
3
4
5
6
7
A
B
C
D
E
φ=0
1-7
φ=15°
1-7
22-28
φ=0
8-14, 22-28
θ 1-4
14-21
φ=45 φ=0
15-21

FIGURE 10

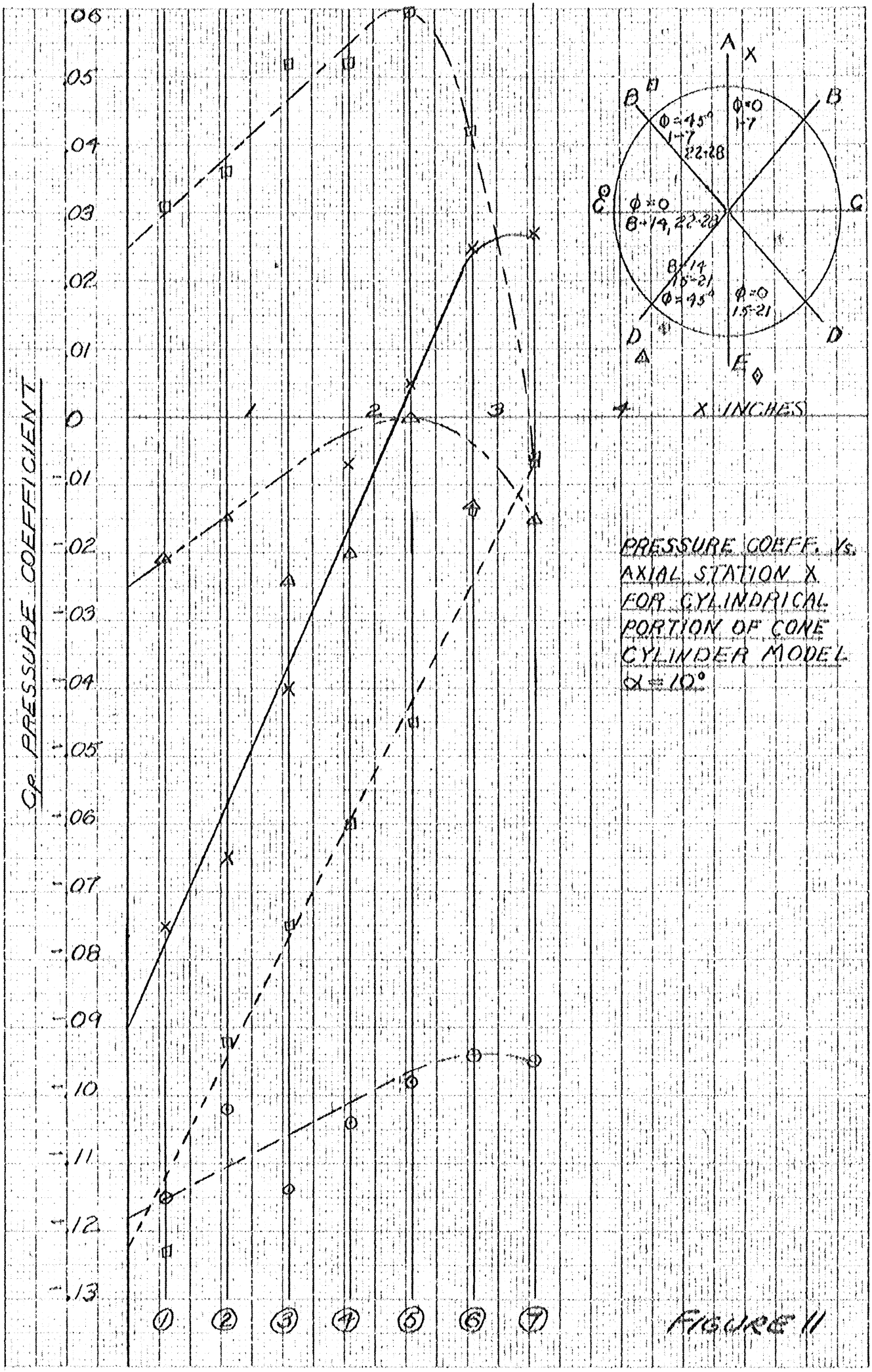

PRESSURE COEFF. Vs. AXIAL STATION X FOR CYLINDRICAL PORTION OF CONE CYLINDER MODEL $\alpha = 10°$

FIGURE 11

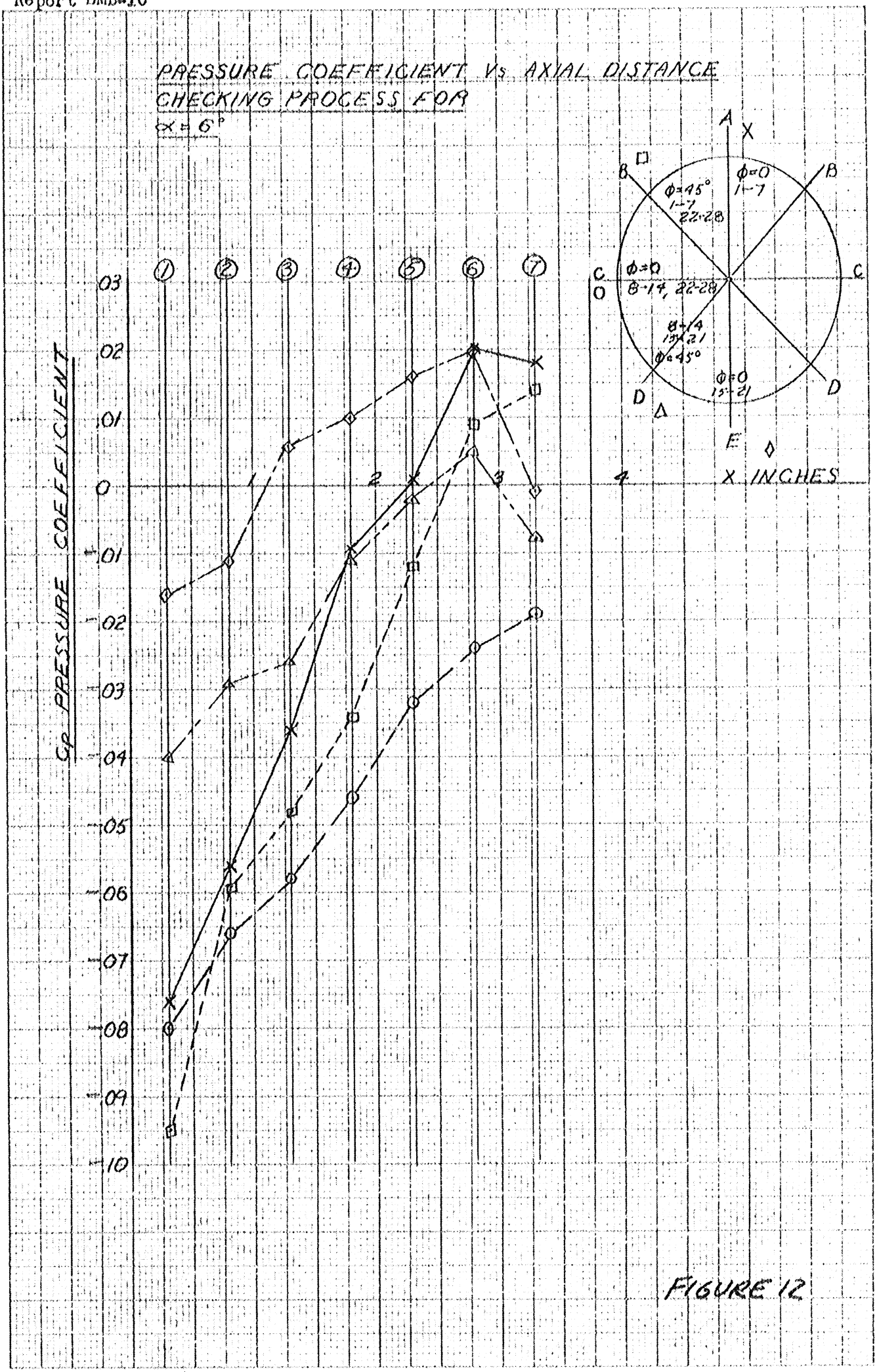
PRESSURE COEFFICIENT Vs AXIAL DISTANCE
CHECKING PROCESS FOR
α = 6°
Cp PRESSURE COEFFICIENT
X INCHES
φ=0
1-7
φ=45°
1-7
22-28
φ=0
8-14, 22-28
8-14
15-21
φ=45°
φ=0
15-21
A
X
B
C
D
E
1
2
3
4
5
6
7

FIGURE 12

COEFFICIENT OF NORMAL FORCE VS ANGLE OF ATTACK FOR CONE-CYLINDER MODEL

Errata: This Figure (5) replaces Figure (5) previously presented as Page 17 in EMB-10

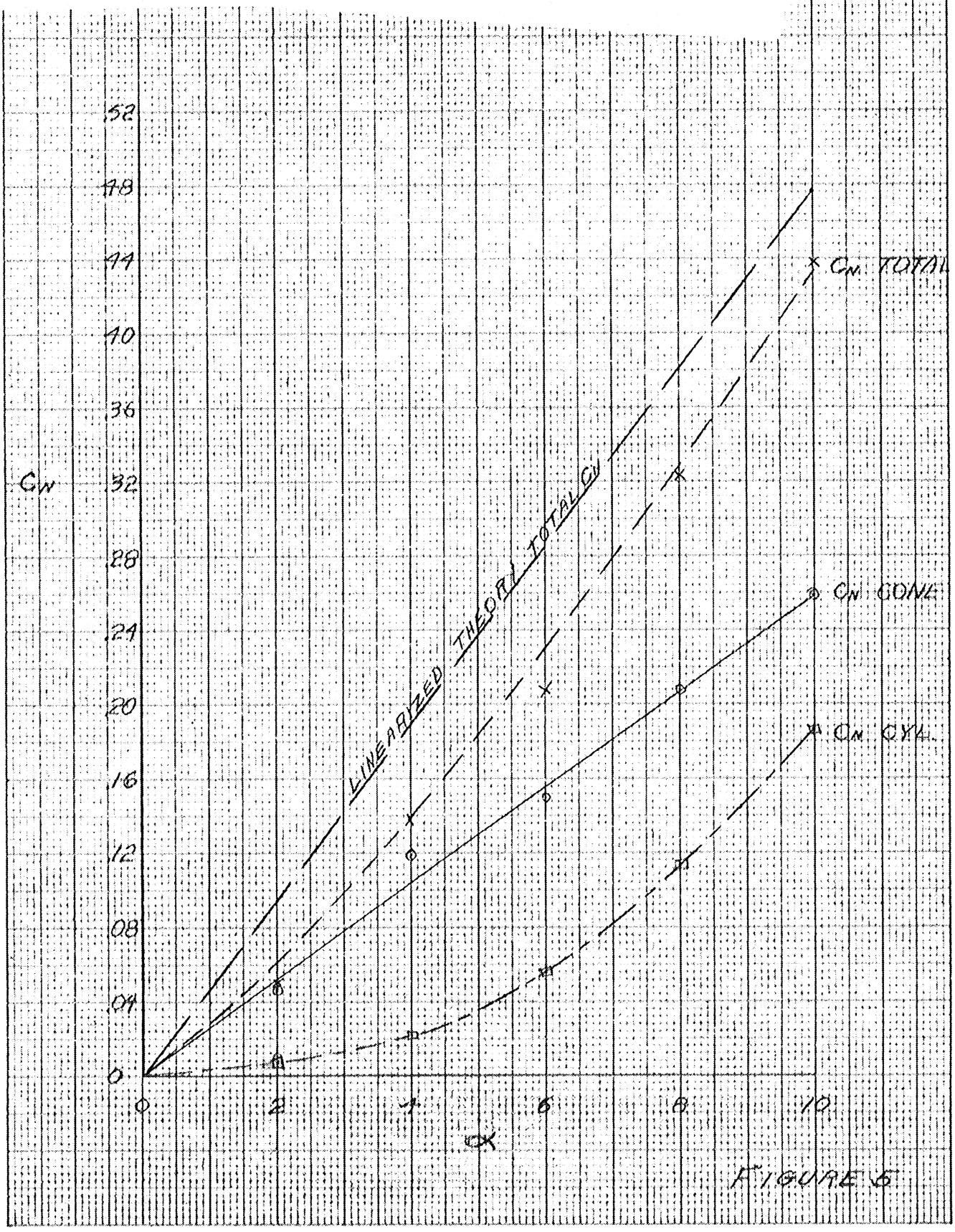

FIGURE 6

COEFFICIENT OF NORMAL FORCE Vs ANGLE OF ATTACK FOR CONE-CYLINDER MODEL

Errata: This Figure (5) replaces Figure (5) previously presented as Page 17 in EMB-10

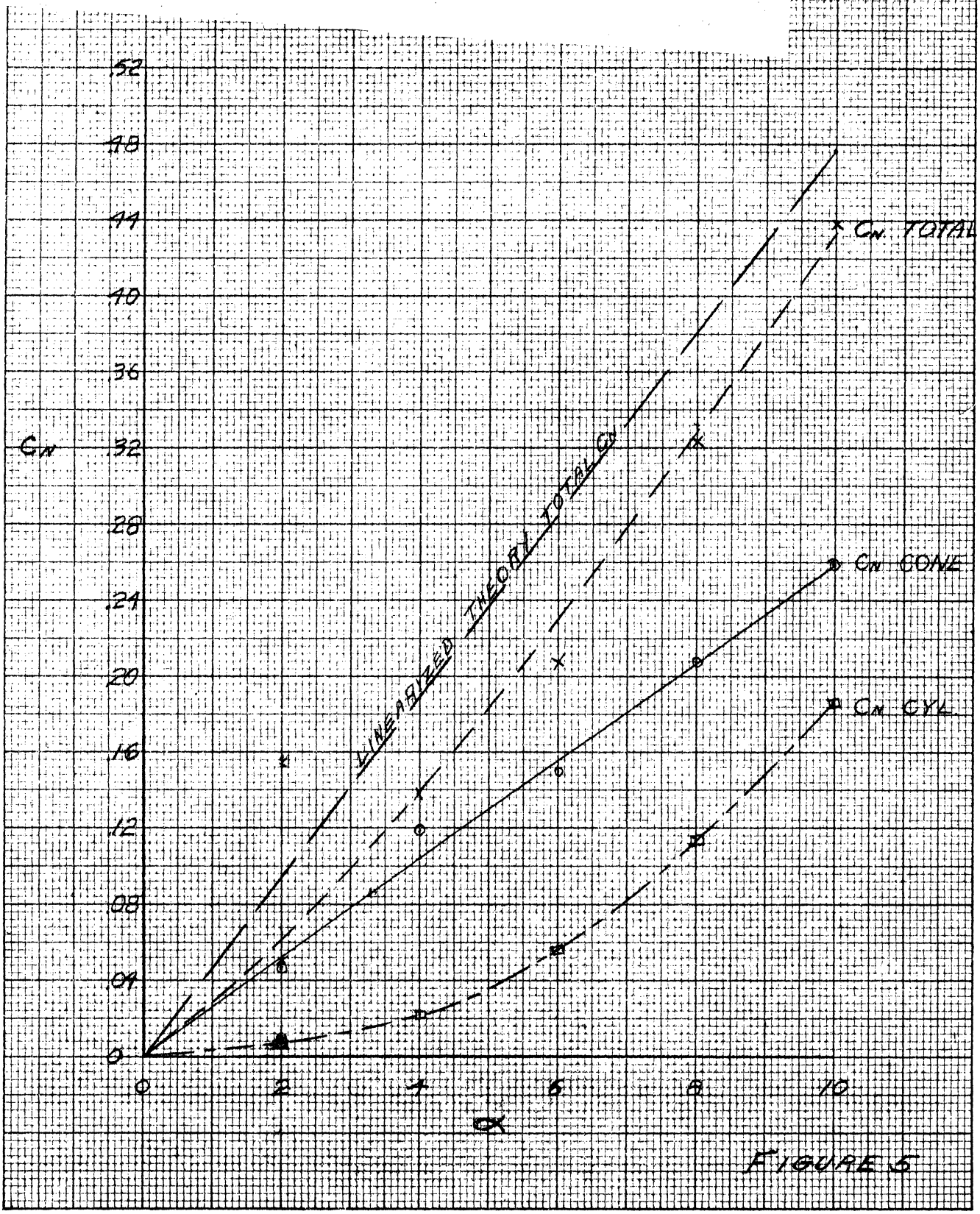

FIGURE 5

COEFFICIENT OF NORMAL FORCE VS ANGLE OF ATTACK FOR CONE-CYLINDER MODEL

Errata: This Figure (5) replaces Figure (5) previously presented as Page 17 in EMB-10

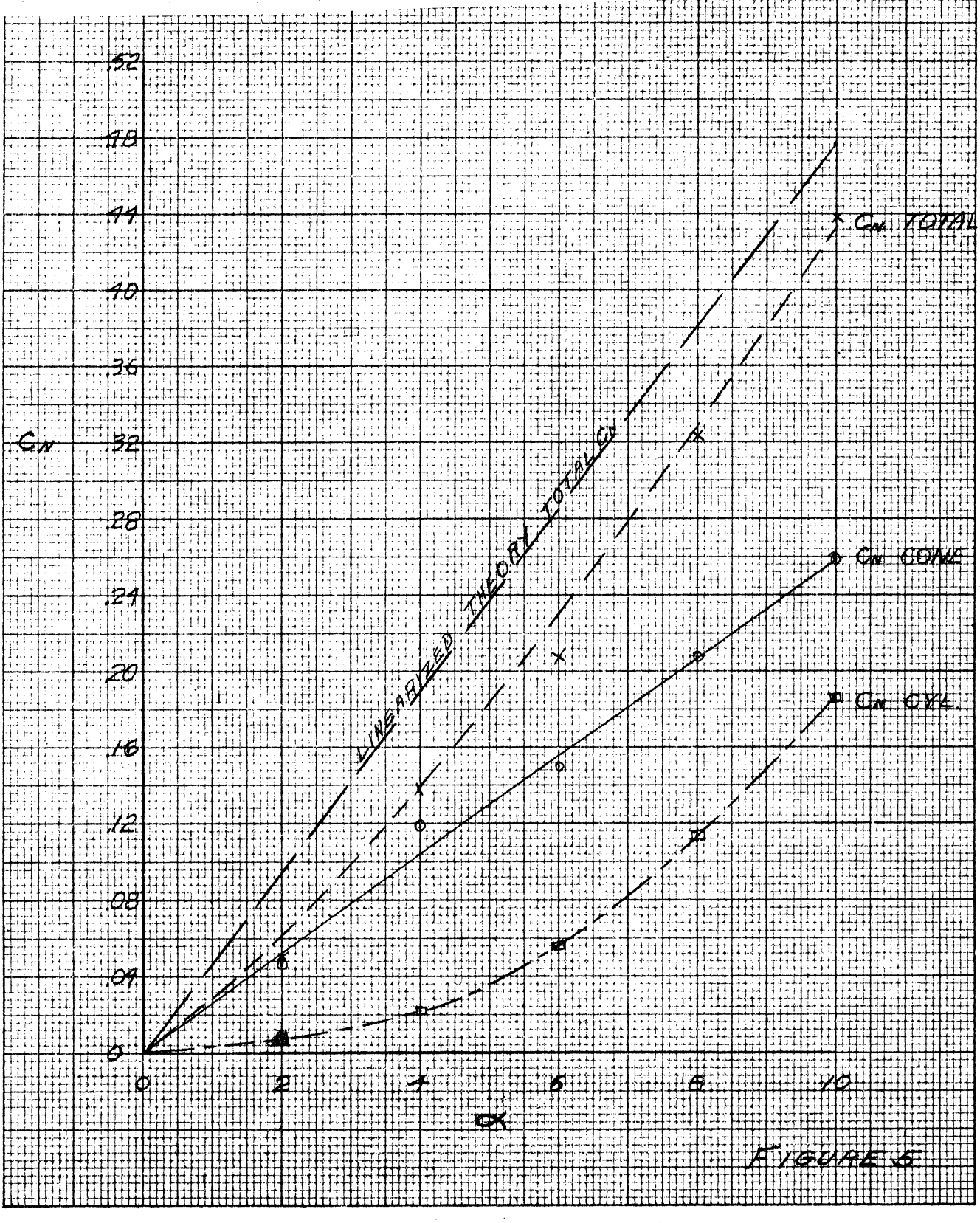

FIGURE 5